01 Dec 2009

Systematic Analysis of Double-Ionization Dynamics Based on Four-Body Dalitz Plots

Daniel Fischer
Missouri University of Science and Technology, fischerda@mst.edu

Michael Schulz
Missouri University of Science and Technology, schulz@mst.edu

Katharina R. Schneider

Marcelo F. Ciappina

et. al. For a complete list of authors, see https://scholarsmine.mst.edu/phys_facwork/793

Recommended Citation

D. Fischer and M. Schulz and K. R. Schneider and M. F. Ciappina and T. Kirchner and A. H. Kelkar and S. Hagman and M. Grieser and K. U. Kuhnel and R. Moshammer and J. H. Ullrich, "Systematic Analysis of Double-Ionization Dynamics Based on Four-Body Dalitz Plots," *Physical Review A - Atomic, Molecular, and Optical Physics*, vol. 80, no. 6, pp. 062703-1-062703-8, American Physical Society (APS), Dec 2009.
The definitive version is available at https://doi.org/10.1103/PhysRevA.80.062703

Systematic analysis of double-ionization dynamics based on four-body Dalitz plots

D. Fischer,[1] M. Schulz,[2] K. Schneider,[1,3] M. F. Ciappina,[4] T. Kirchner,[5] A. Kelkar,[1,3] S. Hagman,[6] M. Grieser,[1] K.-U. Kühnel,[1] R. Moshammer,[1] and J. Ullrich[1]

[1]*Max-Planck-Institut für Kernphysik, Saupfercheckweg 1, 69117 Heidelberg, Germany*

[2]*Physics Department and Laboratory for Atomic, Molecular, and Optical Research, Missouri University of Science and Technology, Rolla, Missouri 65409, USA*

[3]*Extreme Matter Institute EMMI, GSI Helmholtzzentrum für Schwerionenforschung GmbH, Planckstraße 1, 64291 Darmstadt, Germany*

[4]*Institute of High Performance Computing, 1 Fusionopolis Way, No. 16-16 Connexis, 138632 Singapore, Singapore*

[5]*Department of Physics and Astronomy, York University, 4700 Keele Street, Toronto, Ontario, Canada M3J 1P3*

[6]*Gesellschaft für Schwerionenforschung, 64291 Darmstadt, Germany*

(Received 6 October 2009; published 3 December 2009)

We report on an experimental and theoretical systematic study of double ionization of helium by ion impact in terms of four-particle Dalitz plots. Several collision systems covering a broad range of perturbation parameters η (projectile charge to speed ratio) were investigated. With increasing η we observe a systematic trend from features, characteristic to correlated double-ionization mechanisms, to signatures of higher-order processes not requiring electron-electron correlations [the mechanism called "two-step–two projectile-electron interaction" (TS-2)]. The data for the largest η can qualitatively be amazingly well described by a simple model only including the TS-2 mechanism.

DOI: 10.1103/PhysRevA.80.062703 PACS number(s): 34.50.Fa, 34.10.+x

I. INTRODUCTION

Double ionization (DI) of simple atoms by charged particle or photon impact continues to attract widespread interest because the reaction dynamics is distinctly different from single ionization (SI) or other inelastic processes. In particular, electron-electron correlation effects play, at least for specific kinematic conditions, a much more important role than in SI [1]. However, experimentally it is not easy to clearly identify signatures of such correlations because of the complexity of DI. First, there are several different mechanisms contributing to this process, for some of which electron-electron correlation is required, for others it may be relatively unimportant. Second, DI proceeds through a large manifold of forces acting within the six-particle pairs contained in the four-particle collision system (not counting passive electrons, i.e., those not undergoing a transition). Signatures of the electron-electron interaction can thus be easily buried in features resulting from one (or more) of the other five forces.

To some extent it is possible to separate electron-electron correlations from the dynamics of the remaining interactions [2]. Thereby, valuable information has been obtained on the dynamics of the repulsion between the electrons in the final state [2–4] and on initial-state correlations [5,6]. However, this method is not sensitive to the role of electron-electron correlations in the dynamics of the actual transition from the ground state to the double continuum state. To obtain a thorough understanding of electron-electron correlations throughout the entire collision under the influence of the other interactions it is important to study the relative contributions of the different DI mechanisms and the features caused by the forces acting within the various particle pairs.

Three DI mechanisms are usually considered to mostly contribute to the total cross section [1,7–9]. In the first, labeled "two-step–one projectile-electron interaction" (TS-1), only one electron is ejected through a direct interaction with the projectile. This electron then collides in the second step with the other electron lifting it to the continuum. The second mechanism, known as "shake-off" (SO), is very similar to TS-1 in that only one electron is ejected by a direct interaction with the projectile. However, here the second electron gets ejected through rearrangement of the electronic wave function adjusting to a new potential resulting from the ejection of the first electron. Both TS-1 and SO mechanisms are first-order processes in the projectile–target atom interaction and in both some form of electron-electron correlation is required for DI to occur. For simplicity in the following we refer to both of them as TS-1. Finally, in the third mechanism, dubbed "two-step–two projectile-electron interaction" (TS-2), both electrons are ejected through two independent interactions with the projectile. This is a second-order process which does not require (but neither does it rule out) electron-electron correlation.

From measurements of the DI to SI total cross section ratios as a function of projectile energy it has been concluded that DI is dominated by TS-1 at small perturbation parameters η (projectile charge to velocity ratio Q/v_0) [9–11] and by TS-2 at large η [12]. In between both contributions are of similar magnitude and here pronounced interferences between the amplitudes of both processes can be important [9,13]. However, such total cross section measurements are not very sensitive to the details of the collision dynamics. On the other hand, the dominance of TS-1 at small η is also supported by measurements of fully differential cross sections (FDCSs) for double ionization of helium by fast electron impact [14], which offer a much more sensitive test of the theoretical description of the collision dynamics. But here one is confronted with the problem that by their very nature FDCSs only cover a tiny fraction of the total cross section so that features which appear very pronounced in the FDCS may actually be rather insignificant in the overall collision dynamics and vice versa.

To advance our understanding of DI it is desirable to have an analysis tool which combines the sensitivity of FDCS with the comprehensiveness of total cross sections. Such a tool was recently introduced to analyze data on target ionization with simultaneous loss of a projectile electron [15] and later applied to DI [16,17]. In this method, called four-particle Dalitz (4-D) plots, triple differential cross sections are plotted as a function of kinematic parameters of all four collision fragments in a tetrahedral (i.e., a three-dimensional) coordinate system. The integral of a 4-D plot is proportional to the total cross section. 4-D plots thus combine the advantages of FDCS and total cross sections and, in addition, make visible, unlike any other type of plot, the correlation between all final-state particles. This tool has proven its extraordinary power already by demonstrating that at small η (6 MeV p+He collisions) DI is not dominated by TS-1, as taken for granted previously, but by a new mechanism [17]. This process, labeled TS-1–EL, is best viewed as a hybrid process between TS-1 and TS-2. As in TS-1 only one electron is ejected by a direct interaction with the projectile. But as in TS-2 the projectile nevertheless transfers momentum to both electrons in two independent interactions. Apart from the interaction directly ejecting one electron the projectile elastically scatters from the second electron already promoted to the continuum through electron-electron correlation.

To achieve a comprehensive understanding of DI similar data are needed for a broad range of η. After the unexpected realization that TS-1 is not the dominant process at small η further surprises, e.g., that TS-2 may not be dominant at large η, cannot be ruled out. At intermediate η the role of potential interference between the amplitudes for the various DI mechanisms remains to be explored in detail. In this paper we present a systematic analysis of experimental DI data using 4-D plots for η ranging from 0.065 to 5.8. The data for the largest η are compared to several different theoretical calculations, which confirm a dominance of TS-2.

II. EXPERIMENT

The experiments were performed at the 12 MV tandem Van de Graaff accelerator and at the test storage ring (TSR) at the Max-Planck-Institut für Kernphysik in Heidelberg. Well-collimated beams of 6 MeV protons, 24 MeV C^{6+}, and 158 MeV Au^{33+} ions were generated at the 12 MV tandem and 50 MeV C^{6+} and 16 MeV O^{7+} beams at the TSR. At the TSR the ion beams are cooled in a cold bath of electrons moving at equal velocity as the ions. This cooling results in an ion beam size of less than 1 mm and no collimation is needed. The ion beams were intersected with a cold ($T \approx 1-2$ K) atomic helium beam from a supersonic jet.

The ejected electrons and residual recoil ions produced in the collision were extracted by a weak electric field ($U \approx 2.5-4.5$ V/cm) and detected by two-dimensional position-sensitive channel-plate detectors. The electron detector used a delay line anode and could thus be operated in multihit mode, which means that two (or more) electrons ejected in the same event could be detected simultaneously with a single detector. The recoil ions and both electrons were fully momentum analyzed using a standard reaction microscope [18]. Using momentum conservation it is straightforward to show that the momentum transfer $\mathbf{q}$ from the projectile to the target atom is given by $\mathbf{q}=\mathbf{p}_{\mathbf{rec}}+\mathbf{p}_{\mathbf{elec1}}+\mathbf{p}_{\mathbf{elec2}}$, where $\mathbf{p}_{\mathbf{rec}}$ is the recoil-ion momentum and $\mathbf{p}_{\mathbf{elec1}}$ and $\mathbf{p}_{\mathbf{elec2}}$ are the electron momenta.

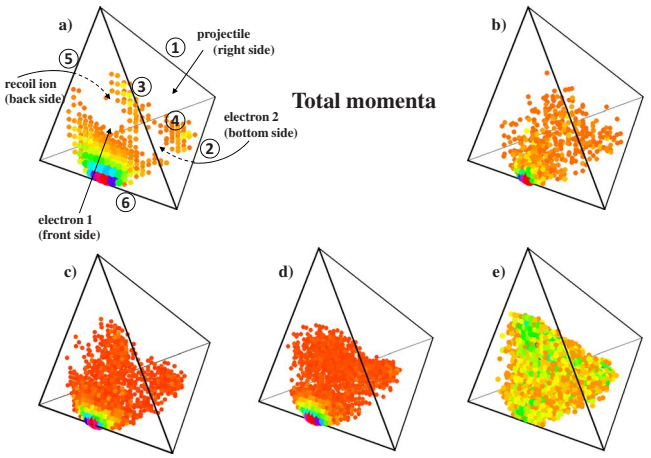

FIG. 1. (Color online) 4-D plots for three-dimensional momenta for double ionization of helium bombarded by (a) 6 MeV p, (b) 50 MeV C^{6+}, (c) 24 MeV C^{6+}, (d) 16 MeV O^{7+}, and (e) 158 MeV Au^{33+}.

The momenta in the longitudinal direction are obtained from a time-of-flight measurement. The reference for this time measurement is provided by the projectile beam pulser. The momentum resolution in this direction is therefore affected by the pulse length. For the experiments at the TSR this pulse length was somewhat longer than at the 12 MV tandem. Here, the overall longitudinal momentum resolutions are about ± 0.1 a.u. for the recoil ions and ± 0.05 a.u. for the electrons, while for the tandem experiments especially the electron resolution was significantly better. The other components are not affected by the pulse length. In the direction perpendicular to both the projectile and target beams (x direction) the resolution is mostly determined by the size of the overlap volume of the two beams and in the target beam direction (y direction) additionally by the target temperature. For the y components the resolutions are ± 0.25 and ± 0.1 a.u. for the recoil ions and the electrons, respectively, and ± 0.1 a.u. for both the recoil ion and the electrons in the x direction. Since the momentum resolution of the electrons is small compared to that of the recoil ion, the momentum transfer resolution is similar to the ones for the recoil ions.

III. EXPERIMENTAL RESULTS AND DISCUSSION

The details of how a 4-D plot is generated have been described earlier [15]. In Fig. 1 such plots are shown for double ionization of He by (a) 6 MeV p (η=0.065), (b) 50 MeV C^{6+} (η=0.47), (c) 24 MeV C^{6+} (η=0.67), (d) 16 MeV O^{7+} (η=1.11), and (e) 158 MeV Au^{33+} (η=5.83) impact. Each tetrahedron plane represents one of the final-state fragments, namely, the front and bottom planes represent the two ejected electrons, the right plane represents the projectile,

and the back plane represents the recoil ion. For a given data point the distances to the four planes provide a set of four relative squared momenta π_i defined as $\pi_i = p_i^2 / \Sigma\, p_j^2$. Here the p_j's are the magnitudes of the momenta of the collision fragments, except for the projectile, where the momentum transfer is used instead.

To illustrate how a 4-D plot should be read consider, e.g., the intersection lines between adjacent planes, which are labeled 1–6 in Fig. 1(a). Data points falling on these lines are at a distance of 0 to the intersecting planes thus corresponding to a momentum of zero of the corresponding particles. For example, at line 1 the planes for the recoil ion and the projectile intersect. For events in that area momentum exchange thus mainly occurs between the two ejected electrons. For the remainder of this paper we refer to interactions leading to a significant momentum exchange between only two particles as binary interactions. With this definition TS-2 can, for example, proceed through a single binary interaction between the projectile and only one electron: although the second electron is directly ejected by the projectile as well, i.e., the projectile transfers enough energy to overcome the binding energy, the momentum transfer is nevertheless essentially zero if that electron is ejected with very small kinetic energy. Binary interactions between the other particle pairs occur at intersection lines 2–6. On the other hand, a data point in the center of the tetrahedron is at an equal distance to all four planes thus representing interactions involving all four particles.

At the smallest perturbation [Fig. 1(a)] strong contributions from binary interactions are quite prominent, where the peak structure at line 6, representing elastic scattering between the heavy particles, is particularly pronounced. This maximum persists to large perturbations; only for the largest η [Fig. 1(e)] the peak structure has vanished. Otherwise, there is a systematic trend that with increasing η the intensity in the 4-D plots increasingly shifts from the intersection lines to the centers of the triangular planes and of the tetrahedron. Therefore, as η rises three- and four-particle interactions become more important in the overall momentum exchange. This is not surprising because the integral of the force that the projectile exerts on the other particles over time increases with η.

The 4-D plots can also be generated for selected directions simply by replacing the p_i and p_j in the computation of the π_i by the corresponding components of these vectors. For the plots shown in Fig. 2 (for the same collision systems as in Fig. 1) this was done for the transverse components in the scattering plane, which is spanned by **q** and the initial projectile momentum (for the remainder of this paper transverse component refers to the one in the scattering plane even when it is not explicitly stated). Likewise, Fig. 3 shows 4-D plots for the longitudinal components (initial projectile beam direction). In contrast to the 4-D plots for the three-dimensional momenta those for the transverse components hardly depend on η at all. For all collision systems they are dominated by binary interactions, as reflected by the peak structures at intersection lines 4–6. Some contributions from four-particle interactions can also be seen in the lower left corner of the tetrahedron. This area represents collisions leading to a large momentum transfer, which is more or less

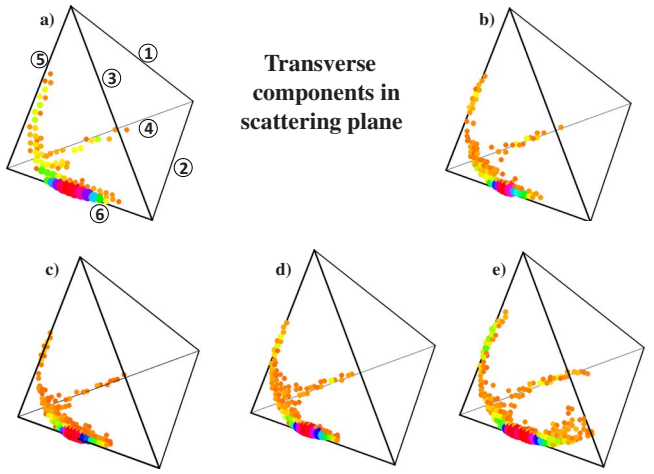

FIG. 2. (Color online) Same as Fig. 1, except the 4-D plots are generated only using the transverse momentum components in the scattering plane for each fragment.

equally shared among the three target fragments. The dominance of binary interactions, even at large η, can be explained as follows: for large projectile velocities the longitudinal component of **q** is small, except for large ejected electron energies. Therefore, the transverse direction nearly coincides with the direction of **q**. At the same time, because of momentum conservation (neglecting the initial internal momentum distribution of the target atom), a binary interaction of the projectile with only one electron or with the recoil ion leads to $\mathbf{p}_{\mathbf{elec}} = \mathbf{q}$ (intersection lines 4 and 5) or $\mathbf{p}_{\mathbf{rec}} = \mathbf{q}$ (intersection line 6). As a result binary interactions involving the projectile contribute mostly to the transverse direction. For multiple particle interactions, in contrast, momentum conservation does not link the direction of the electron and recoil-ion momenta to **q** and events emerging from such interactions are more uniformly distributed in all directions. Indeed, in the 4-D plots for the three-dimensional momenta binary interactions are much less pronounced.

In the 4-D plots for the longitudinal direction (Fig. 3) binary interactions involving the projectile are much less im-

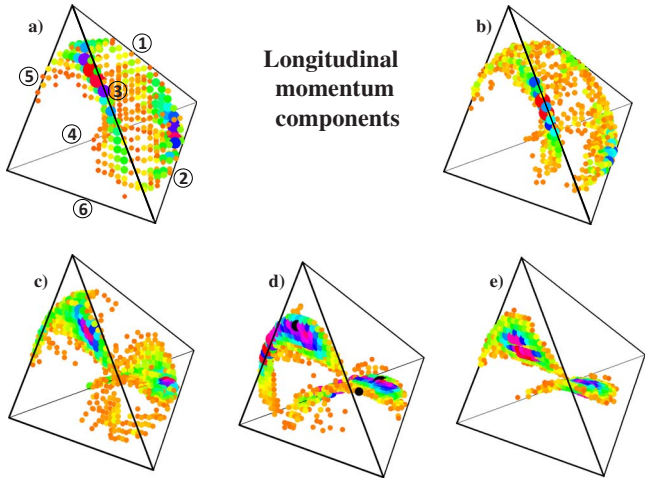

FIG. 3. (Color online) Same as Fig. 1, except the 4-D plots are generated only using the longitudinal momentum components for each fragment.

portant than in the transverse direction as well, in accord with the above arguments. Also, here the overall momentum exchange is much more sensitive to η. Although the plots are quite similar for $\eta \lesssim 0.5$ [Figs. 3(a) and 3(b)] and again for $\eta \gtrsim 1$ [Figs. 3(d) and 3(e)] the plots for the small-η regime look qualitatively very different from those for the large-η regime. For $\eta \lesssim 0.5$ pronounced peak structures representing binary recoil-ion–electron interactions (intersection lines 2 and 3) are observed. In general, most of the intensity is close to the projectile plane so that here DI is dominated by collisions leading to small longitudinal momentum transfers q_z. This can be understood from simple kinematics: applying energy and momentum conservations it can be shown that to a very good approximation

$$q_z = (I + E_{\mathrm{elec1}} + E_{\mathrm{elec2}})/v_0, \tag{1}$$

where I is the DI potential of 79 eV. Therefore, q_z is small at large v_0, except for large ejected electron energies (e.g., for 6 MeV p+He, $E_{\mathrm{elec1}}+E_{\mathrm{elec2}}<50$ eV, $q_z<0.3$ a.u.).

At large η the longitudinal 4-D plots exhibit very different features compared to small η. The contributions from binary recoil-ion electron interactions are now rather insignificant. For O^{7+}+He collisions [Fig. 3(d)] binary projectile–electron interactions (intersection lines 4 and 5) are now quite pronounced instead. But the dominant feature, especially for the Au^{33+} projectiles [Fig. 3(e)], is a "shoe-tongue-like" distribution located on both electron planes. Near the centers of these planes the "shoe-tongues" bend toward the center of the tetrahedron. These regions correspond to three-particle interactions between one electron, which has the largest momentum, the recoil ion, and the projectile. The areas where the shoe-tongues bend demonstrate that even four-particle interactions are present, although here the intensity is rather weak.

A detailed analysis of the longitudinal 4-D plots for large η shows that the signatures seen in these plots are due to a strong postcollision interaction (PCI) between the outgoing projectile and one (or both) of the ejected electrons. PCI can result in a focusing of the projectile and the electron(s) toward the initial projectile beam axis [19] and, in its most drastic manifestation, in cusp-electron production, i.e., electrons which move at the same speed and in the same direction as the projectiles [20]. The location of such events in a 4-D plot can be estimated by calculating q_z from Eq. (1) and the longitudinal component of the recoil-ion momentum p_{recz} from momentum conservation if the electron momenta are given. For example, the two black dots on the electron planes in Fig. 3(d) indicate the location of events where one electron is moving parallel and the second electron perpendicular to the projectile beam (i.e., assuming that only one electron experiences strong PCI), both with a speed of 1 a.u. This location changes hardly at all if the speed of the electron moving parallel to the projectile is changed to the projectile speed (6.32 a.u.). Also, for the Au^{33+} projectiles one finds essentially the same locations.

The black point closest to the tetrahedron center indicates the location of events where both electrons are moving parallel to the projectile beam (i.e., assuming that both electrons experience strong PCI) with a speed of 1 a.u. Here, the intensity is very small because the Coulomb repulsion prohibits events where both electrons are moving at the same velocity vector. However, if the areas of the main intensity in both bending shoe-tongues are extrapolated toward the center of the tetrahedron the point representing both electrons moving along the beam axis is located precisely where these extrapolations meet. The bending of the shoe-tongues can therefore be interpreted in terms of PCI trying to force both electrons toward the beam axis, but the Coulomb repulsion partially counteracting this tendency.

The large contributions from binary projectile–electron interactions (intersection lines 4 and 5) for the O^{7+} projectiles can be explained, at least partly, in terms of PCI strongly affecting only one electron as well. Although, as mentioned above, the location of such events in the 4-D plots does not change significantly as the speed of the electron moving parallel to the projectile beam varies between approximately 1 a.u. and v_0, this is not the case for electron speeds smaller than 1 a.u. For example, if the speed of both electrons is 0.5 a.u. (with one electron moving parallel and the second perpendicular to the projectile beam) q_z happens to be almost identical to the electron speed [see Eq. (1)]. Due to momentum conservation p_{recz} is then zero and such events are consequently located on intersection lines 4 and 5 in the 4-D plot. The term "binary interaction" may be a little bit misleading in this case as it may suggest that the recoil ion is passive. However, the recoil ion does take an active role in PCI and its zero longitudinal momentum is merely due to a coincidental cancellation of the momentum exchange with the electron and the projectile which happens to occur for an electron speed around 0.5 a.u.

For the Au^{33+} projectiles PCI is even much stronger than for O^{7+}. As a result the electrons are not only more tightly focused to the beam axis, but they are also more strongly accelerated in the forward direction by the projectiles. Therefore, the relative intensity of electrons with a longitudinal speed of less than 1 a.u. is much smaller than for O^{7+} leading to a much weaker intensity near intersection lines 4 and 5. This explanation is supported by the longitudinal 4-D plot generated under the condition that both electron momenta are smaller than 1 a.u., which is shown in Fig. 4(a). Here, the electrons are distinguished by their direction relative to the beam axis: electron 1, represented by the front plane of the tetrahedron, is defined to be the one for which the angle between its momentum vector and the initial projectile beam direction is smaller than for electron 2 (bottom plane). The total number of counts in this spectrum is indeed much more reduced by the condition than in the corresponding plot for the O^{7+} projectiles. More importantly, for the remaining intensity a pronounced peak structure is now observed near intersection line 4, which is exactly the signature expected for electron 1 being strongly affected by PCI. In contrast, almost no intensity at all is observed near intersection line 5 because electron 2, i.e., the electron which is less focused toward the beam axis, is much less affected by PCI. Without a strong effect of PCI on either electron, on the other hand, one would expect that the condition should lead to large contributions near intersection line 6 because it only forces the longitudinal electron momenta, but not q_z and p_{recz}, to be small. This expectation is confirmed by our theoretical analysis, as we will show below.

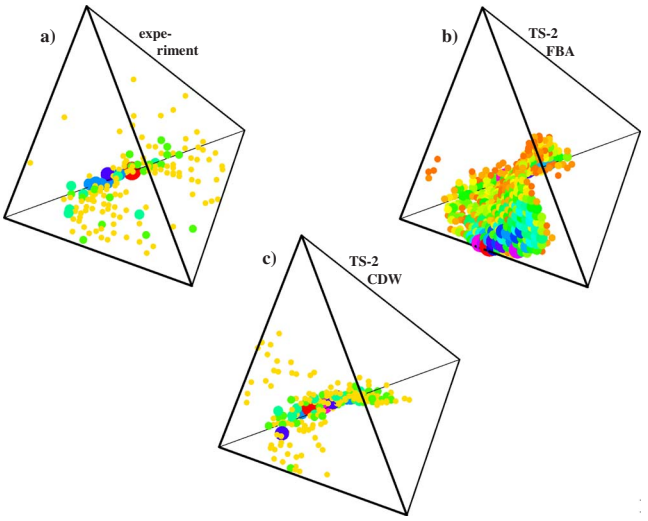

FIG. 4. (Color online) 4-D plots for the longitudinal momentum components for 158 MeV Au^{33+}+He collisions with the condition that the energy of both ejected electrons is smaller than 15 eV. (a) Experimental data, (b) TS-2–FBA calculation, and (c) TS-2–CDW calculation.

IV. COMPARISON TO THEORY

The computation of 4-D plots is numerically very demanding. To obtain an n-fold differential cross section in principle involves an integration of the FDCS (eightfold differential) over $8n$ momentum components (in addition to the spatial integral required to calculate the FDCS), which to a large extent has to be done numerically. Often, the dimension of the integral can be reduced by taking advantage of symmetries using appropriate coordinates. Unfortunately, for the 4-D plots the degree of symmetry that could be exploited is rather limited if present at all. A calculation of these plots by a direct integration of the FDCS therefore does not seem feasible with current computer power. This problem has been circumvented by using the Monte Carlo event generator (MCEG) technique [21,22]. In this method an event file, similar to the data files of a multiparameter coincidence measurement, is produced based on theoretical FDCS. Any cross section can then be generated by sorting the events into histograms, using appropriate conditions, in exactly the same manner as used in extracting the cross section from the data of a kinematically complete experiment. With this technique the computation of 4-D plots has become possible [16,17], however, the generation of the event file is still very time intensive even when utilizing a large number of processors. Therefore, this method is limited to relatively simple models for which the computation of the FDCS is not already numerically too intensive.

The first theoretical 4-D plots were obtained for 6 MeV p+He collisions [16], i.e., for the smallest η we studied so far, using two different models. One calculation was based on the first Born approximation (FBA) using a correlated wave function for the initial state and the Gamow factor to account for final-state correlation. This approach seemed reasonable since TS-1 was thought to be the dominant process for such small η. Although expected to be negligible, 4-D plots were also calculated for the pure TS-2 contributions. This was done by convoluting the cross sections for single ionization of He and of He^+. Later, contributions from the TS-1–EL process were accounted for by convoluting the theoretical TS-1 cross sections with classical elastic scattering between the projectile and the electron which was ejected through electron-electron correlation [17]. Although the TS-1–EL calculation was in nice qualitative agreement with the experimental data, one weakness of this approach is that TS-1 and TS-1–EL are not treated coherently. For intermediate η this problem becomes more severe because here TS-2 contributions are of similar magnitude as those from TS-1 and TS-1–EL. However, the TS-2 calculation is based on a convolution of single ionization cross sections rather than amplitudes. Therefore, using this simplified model for TS-2 it cannot be treated coherently with TS-1. On the other hand, at the largest η studied here, i.e., for the Au^{33+} projectiles, TS-2 is expected to be dominant and the cross term between the various amplitudes should be small. In the following we therefore compare the experimental data for this collision system to various theoretical models with a special emphasis on TS-2 calculations.

The theoretical models and the MCEG technique have been described in detail previously [16,21,22] and only the salient points are repeated here, and modifications to account for features, characteristic to this large perturbation collision system, are emphasized. The TS-2 process is modeled by convoluting the FDCS for single ionization of He and of He^+ with each other. Two separate TS-2 calculations were performed: in one, labeled TS-2–FBA, the FDCS for each SI step was calculated within the FBA and in the other, labeled TS-2–CDW, within the continuum-distorted-wave–eikonal-initial-state (CDW-EIS) approach [23]. In all models presented here the projectile–target nucleus interaction was not accounted for in the calculation of the FDCS but was included in the generation of the 4-D plots by convoluting the FDCS with classical elastic scattering [16,24]. The Coulomb repulsion between the two ejected electrons is accounted for in terms of the Gamow factor [16]. The main difference between the TS-2–FBA and TS-2–CDW calculations is that in the latter PCI is included in the final-state wave function in the calculation of the FDCS for each SI step. To test the sensitivity of the 4-D plots on the specific DI mechanism, we also compare the data to TS-1 and TS-1–EL calculations. In both models the FDCSs for DI were calculated within the FBA [16]. The TS-1–EL results are obtained by convoluting the FDCS for TS-1 with classical elastic scattering between the projectile and the slower of the two ejected electrons, as described earlier [17].

In Fig. 5 the experimental [panel (a)] and theoretical 4-D plots for the three-dimensional momenta are compared for Au^{33+}+He collisions. The theories are [panel (b)] TS-1, [panel (c)] TS-2–FBA, [panel (d)] TS-1–EL, and [panel (e)] TS-2–CDW. None of the calculations is in satisfactory agreement with the data and it is not even possible to single out one model as being favored by the data over the others. These theoretical difficulties are not entirely unexpected. The involvement of two active electrons makes DI a significantly more complex process than SI to begin with. The strong higher-order contributions at this large η, not just the grow-

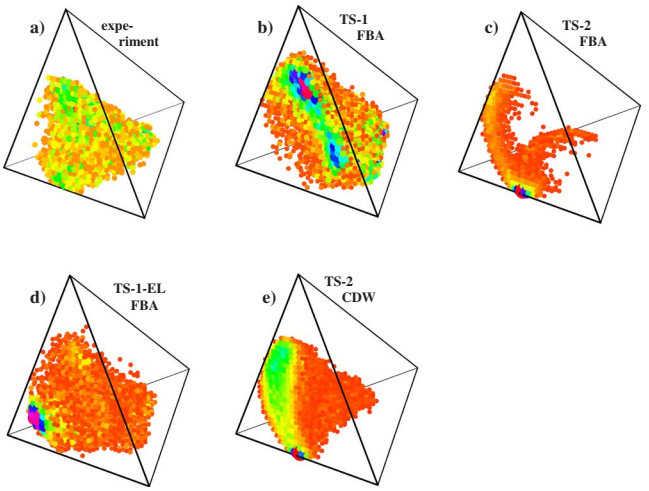

FIG. 5. (Color online) Comparison between experiment and theory for 158 MeV Au^{33+}+He collisions of the 4-D plots for the three-dimensional momenta. (a) Experimental data, (b) TS-1 calculation, (c) TS-2–FBA calculation, (d) TS-1–EL calculation, and (e) TS-2–CDW calculation.

ing importance of TS-2 but also increasing higher-order contributions to the ejection of a single electron (especially PCI), make accurate calculations extremely difficult.

Even for the much smaller η for p+He collisions only limited success in describing the 4-D plots for the three-dimensional momenta was achieved [16]. In contrast, there nice qualitative agreement with the experimental 4-D plots for the transverse and longitudinal components was obtained. Here, we encounter a similar situation for Au^{33+}+He collisions, for which the 4-D plots are shown (in the same order as in Fig. 5) in Fig. 6 for the transverse components and in Fig. 7 for the longitudinal components. In both cases the data are well reproduced by the TS-2–CDW model. The TS-1 model, in contrast, is in poor agreement with the data. In the plots for the transverse components the TS-1–EL approach leads to somewhat improved agreement compared to the TS-1 model, but considerable discrepancies nevertheless remain. The TS-2–FBA model, on the other hand, describes the experimental 4-D plot equally well (or even better) as the TS-2–CDW calculation. The 4-D plots for the transverse direction are thus consistent with a dominance of TS-2 expected for double ionization at such large η, but they are not at all sensitive to PCI.

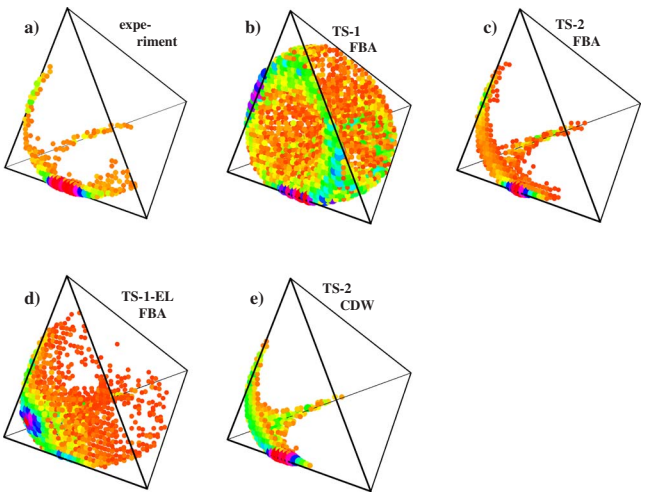

FIG. 6. (Color online) Same as Fig. 5 for transverse momentum components in the scattering plane.

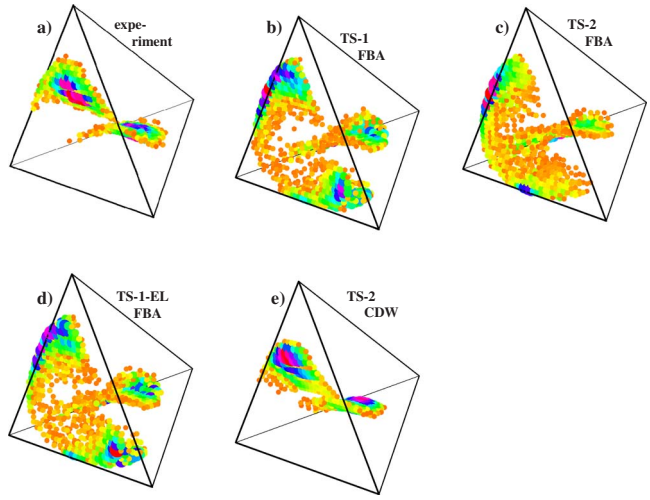

FIG. 7. (Color online) Same as Fig. 5 for longitudinal momentum components.

In sharp contrast to the transverse direction the 4-D plots for the longitudinal components clearly demonstrate a strong role of PCI. Here, the TS-2–FBA calculation is in equally poor agreement with the data and the TS-2–CDW model as the TS-1 and TS-1–EL calculations. The strong effect of PCI even on low-energy electrons is also confirmed by our calculations. As mentioned above, in the longitudinal 4-D plots with the condition that the momenta of both ejected electrons are less than 1 a.u. (Fig. 4) one would expect strong contributions near intersection line 6 in the absence of PCI. This is indeed seen in our TS-2–FBA calculation [Fig. 4(b)]. In the TS-2–CDW model [Fig. 4(c)], in contrast, these contributions are almost completely missing and the plot is now dominated by a peak structure at intersection line 4, in accordance with the experimental data.

Before concluding, based on the comparison between the data and our theoretical calculations, that the signatures of TS-2 are manifested in the 4-D plots at large η, it is important to test that other spectra can also be at least qualitatively reproduced by our TS-2–CDW model. In the case of 6 MeV p+He collisions (where PCI is insignificant) the measured 4-D plot for the transverse direction was well reproduced by a TS-2–FBA calculation [17]. However, at the same time serious discrepancies were found in the fourfold differential cross sections (4DCSs) for electrons of equal energy ejected into the scattering plane to measured data reported earlier [25]. The simultaneous analysis of the 4-D plots and the 4DCS proved to be crucially important. It led to the conclusion that the features observed in the 4-D plots were actually signatures of the TS-1–EL process, which for this collision system happened to be very similar to those of TS-2. Although for Au^{33+}+He collisions the 4-D plots calculated with the TS-1, TS-1–EL, and TS-2–CDW models are all very different, successfully testing theory in terms of the 4DCS nev-

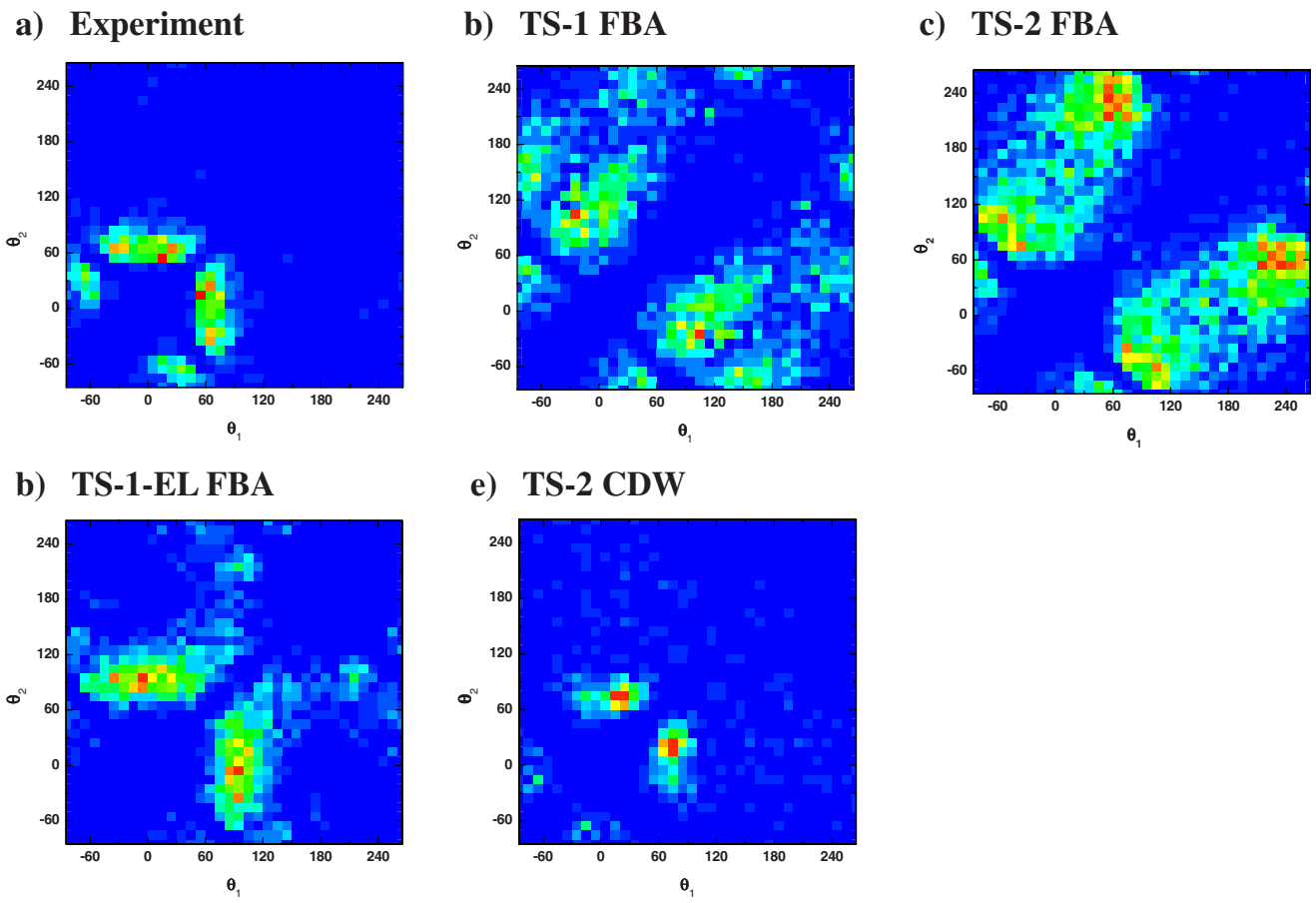

FIG. 8. (Color online) 4DCS for electrons of equal energy ejected into the scattering plane as a function of the ejection angle of both electrons for 158 MeV Au^{33+}+He collisions. (a) Experimental data, (b) TS-1 calculation, (c) TS-2–FBA calculation, (d) TS-1–EL calculation, and (e) TS-2–CDW calculation.

ertheless raises the confidence level in the analysis of the 4-D plots. In Fig. 8 4DCSs measured for this collision system [panel (a)] are plotted as a function of the ejection angles of both electrons and compared to TS-1 [panel (b)], TS-2–FBA [panel (c)], TS-1–EL [panel (d)], and TS-2–CDW [panel (e)] calculations. Indeed, the best agreement with the data is achieved with the TS-2–CDW model and, not surprisingly, severe discrepancies are observed with the TS-1 and TS-2–FBA approaches.

V. CONCLUSIONS

We have presented a systematic study of double ionization in terms of 4-D plots covering a broad range of perturbation parameters η. One important advantage of this method is that multiple differential cross sections as a function of the momenta of all collision fragments are presented in a single spectrum without loss of any part of the total cross section. Earlier, we demonstrated the extraordinary power of this method by identifying a new double-ionization mechanism [17], which is important at small η. Here, we demonstrated that the 4-D plots reveal how, starting at small η, features, characteristic to TS-1–EL with increasing η, systematically develop into signatures of the TS-2 process. The 4-D plots for the longitudinal components are also very sensitive to PCI, which becomes increasingly important with increasing η. Only the 4-D plots for the transverse components hardly depend on η at all. The comparison to theory shows that this weak dependence is due to a remarkable insensitivity of the TS-2 signatures on η combined with a strong resemblance of TS-1–EL with TS-2 at small η, where TS-1–EL is dominant.

Although the theoretical models that the data are compared to are relatively simple the 4-D plots for the transverse and longitudinal components are amazingly well produced by the TS-2–CDW calculation considering the complexity of the double-ionization dynamics. This success illustrates both the strength of the analysis of 4-D plots and its limitations: on one hand, the basic features of the data can be well described as long as the theoretical model makes reasonable assumptions about the underlying basic reaction dynamics. Since these features do not seem to be very sensitive to the technical details of the calculation the dominant double-ionization mechanism can be identified without the analysis being significantly compromised by the limitations of the model. On the other hand, this restricted sensitivity also means that the 4-D plots are not very suitable to perform a detailed test of theory on a quantitative level.

The observation that the 4-D plots for the three-dimensional momenta are not well reproduced by theory, although those for the individual components are well de-

scribed by the TS-2–CDW model, suggests that the interdependence between the various components is not reproduced by the calculations. A similar trend was also observed for 6 MeV p+He collisions. Nevertheless, analyzing the 4-D plots for the individual components appears to be a powerful tool to study the double-ionization dynamics in great detail. It should also be noted that the relatively simple models presented here only mark the beginning of a potentially fruitful development. We are currently working on a more sophisticated model which includes all double-ionization mechanisms discussed here (TS-1, TS-1–EL, and TS-2) simultaneously and treats them coherently. We will apply this model to perform calculations for the collision systems corresponding to intermediate η. Furthermore, with the still rapidly growing computer power it should become feasible in the foreseeable future to generate event files with numerically much more intensive and refined models. 4-D plots may then even offer a quantitative test of theory.

ACKNOWLEDGMENTS

We are grateful for support by the Alliance Program of the Helmholtz Association (HA216/EMMI), by the German Research Foundation (DFG) within the Emmy Noether program under Contract No. FI 1593/1-1, and by the National Science Foundation under Grant No. PHY0652519. We would like to thank the Max-Planck-Institut für Physik Komplexer Systeme for letting us use their computational facilities.

[1] J. H. McGuire, *Electron Correlation Dynamics in Atomic Collisions* (Cambridge University Press, Cambridge, 1997).
[2] M. Schulz, R. Moshammer, W. Schmitt, H. Kollmus, B. Feuerstein, R. Mann, S. Hagmann, and J. Ullrich, Phys. Rev. Lett. **84**, 863 (2000).
[3] L. G. Gerchikov and S. A. Sheinerman, J. Phys. B **34**, 647 (2001).
[4] L. Gulyás, A. Igarashi, and T. Kirchner, Phys. Rev. A **74**, 032713 (2006).
[5] M. Schulz, R. Moshammer, L. G. Gerchikov, S. A. Sheinerman, and J. Ullrich, J. Phys. B **34**, L795 (2001).
[6] L. G. Gerchikov, S. A. Sheinerman, M. Schulz, R. Moshammer, and J. Ullrich, J. Phys. B **35**, 2783 (2002).
[7] M. H. Mittleman, Phys. Rev. Lett. **16**, 498 (1966).
[8] F. W. Byron and C. J. Joachain, Phys. Rev. Lett. **16**, 1139 (1966).
[9] J. H. McGuire, Phys. Rev. Lett. **49**, 1153 (1982).
[10] H. K. Haugen, L. H. Andersen, P. Hvelplund, and H. Knudsen, Phys. Rev. A **26**, 1962 (1982).
[11] B. L. Schram, A. J. H. Boerboom, and J. Kistemaker, Physica (Utrecht) **32**, 185 (1966).
[12] H. Knudsen, L. H. Andersen, P. Hvelplund, G. Astner, H. Cederquist, H. Danared, and L. Liljeby, J. Phys. B **17**, 3545 (1984).
[13] L. H. Andersen, P. Hvelplund, H. Knudsen, S. P. Møller, K. Elsener, K.-G. Rensfelt, and E. Uggerhøj, Phys. Rev. Lett. **57**, 2147 (1986).
[14] A. Dorn, A. Kheifets, C. D. Schröter, B. Najjari, C. Höhr, R. Moshammer, and J. Ullrich, Phys. Rev. Lett. **86**, 3755 (2001).
[15] M. Schulz, D. Fischer, T. Ferger, R. Moshammer, and J. Ullrich, J. Phys. B **40**, 3091 (2007).
[16] M. F. Ciappina, M. Schulz, T. Kirchner, D. Fischer, R. Moshammer, and J. Ullrich, Phys. Rev. A **77**, 062706 (2008).
[17] M. Schulz, M. F. Ciappina, T. Kirchner, D. Fischer, R. Moshammer, and J. Ullrich, Phys. Rev. A **79**, 042708 (2009).
[18] R. Moshammer, M. Unverzagt, W. Schmitt, J. Ullrich, and H. Schmidt-Böcking, Nucl. Instrum. Methods Phys. Res. B **108**, 425 (1996).
[19] T. Vajnai, A. D. Gaus, J. A. Brand, W. Htwe, D. H. Madison, R. E. Olson, J. L. Peacher, and M. Schulz, Phys. Rev. Lett. **74**, 3588 (1995).
[20] G. B. Crooks and M. E. Rudd, Phys. Rev. Lett. **25**, 1599 (1970).
[21] M. Dürr, B. Najjari, M. Schulz, A. Dorn, R. Moshammer, A. B. Voitkiv, and J. Ullrich, Phys. Rev. A **75**, 062708 (2007).
[22] M. F. Ciappina, T. Kirchner, and M. Schulz (unpublished).
[23] D. S. F. Crothers and J. F. McCann, J. Phys. B **16**, 3229 (1983).
[24] M. Schulz, M. Dürr, B. Najjari, R. Moshammer, and J. Ullrich, Phys. Rev. A **76**, 032712 (2007).
[25] D. Fischer, R. Moshammer, A. Dorn, J. R. Crespo López-Urrutia, B. Feuerstein, C. Höhr, C. D. Schröter, S. Hagmann, H. Kollmus, R. Mann, B. Bapat, and J. Ullrich, Phys. Rev. Lett. **90**, 243201 (2003).